



## Seizure localization using EEG analytical signals

Mark H. Myers<sup>a,\*</sup>, Akaash Padmanabha<sup>b</sup>, Gavin M. Bidelman<sup>a,c,d</sup>, James W. Wheless<sup>e</sup>

<sup>a</sup> Department of Anatomy and Neurobiology, University of Tennessee Health Sciences Center, Memphis, TN, USA

<sup>b</sup> Department of Chemical Engineering, University of Pennsylvania, Philadelphia, PA, USA

<sup>c</sup> Institute for Intelligent Systems, University of Memphis, Memphis, TN, USA

<sup>d</sup> School of Communication Sciences & Disorders, University of Memphis, Memphis, TN, USA

<sup>e</sup> Department of Neurology, University of Tennessee Health Science Center, Memphis, TN, USA



### ARTICLE INFO

#### Article history:

Accepted 25 May 2020

Available online 25 June 2020

#### Keywords:

Analytic amplitude (AA)

Analytic phase (AP)

Seizure onset zone (SOZ)

Electroencephalograph (EEG)

### HIGHLIGHTS

- Continuous monitoring of phase & energy of EEG signals to perform source location.
- Methodology was found to be robust in locating short seizure instances (8–12 sec).
- Algorithm achieved 93.3% precision and accuracy and 100% sensitivity.

### ABSTRACT

**Objective:** Localization of epileptic seizures, usually characterized by abnormal hypersynchronous wave patterns from the cortex, remains elusive. We present a novel, robust method for automatic localization of seizures on the scalp from clinical electroencephalogram (EEG) data.

**Methods:** Seizure patient EEG data was decomposed via the Hilbert Transform and processed through the following methodology: sorting the analytic amplitude (AA) in the time instance, locating the maximum amplitude within the vector of channels, cross-correlating amplitude values in the time index with the channel vector. The channel with highest AA value in time was located.

**Results:** Our approach provides an automated way to isolate the epi-genesis of seizure events with 93.3% precision and 100% sensitivity. The method differentiates seizure-related neural activity from other common EEG noise artifacts (e.g., blinks, myogenic noise).

**Conclusions:** We evaluated performance characteristics of our source location methodology utilizing both phase and energy of EEG signals from patients who exhibited seizure events. Feasibility of the new algorithm is demonstrated and confirmed.

**Significance:** The proposed method contributes to high-performance scalp localization for seizure events that is more straightforward and less computationally intensive than other methods (e.g., inverse source modeling). Ultimately, it may aid clinicians in providing improved patient diagnosis.

© 2020 International Federation of Clinical Neurophysiology. Published by Elsevier B.V. All rights reserved.

## 1. Introduction

Epileptic seizures are a dysfunction in the brain that are characterized by simultaneous and periodic firing of large neural populations (Shoeb et al., 2004). Rapid localization of seizures is critical in medical environments to notifying medical staff and prevent further patient complications. Automatic localization of seizure events from EEG signals has been examined in several previous

studies using a variety of approaches including machine learning (Shoeb and Gutttag, 2010), frequency transforms (Hartmann et al., 2011), and nonlinear association analysis (Westmijse et al., 2009).

Knowledge about the exact seizure onset zone (SOZ) is of utmost importance for planning surgical treatment of epilepsy (Boon and D'Have, 1995; Boon et al., 1997). This task can be accomplished using either invasive or non-invasive methods. The problem is finding the exact location of the source of the seizure from the projections of electrodes scattered on the scalp. Although invasive methods (e.g., intracranial recordings) are generally more accurate and reliable because of the higher signal-to-noise ratio (SNR) of the signals, the higher risk of infection and the high cost

\* Corresponding author at: Department of Anatomy and Neurobiology, University of Tennessee Health Sciences Center, Memphis, TN 38163, USA.

E-mail address: [mhmyers99@gmail.com](mailto:mhmyers99@gmail.com) (M.H. Myers).

of performing the required operations necessitates the exploration of alternative methods like the scalp EEG. A comprehensive review of the available methods is presented in Michel et al. (2004). The two most common approaches to EEG source analysis are the parametric beamformer method and non-parametric LORETA method.

The beamformer enables source localization by suppressing interfering activity of neighboring neural regions from the region of interest through spatial filtering. Source locations are found through dipole modelling, where the parameters used are location and orientation. A series of dipoles represents the spatial alignment across the brain. There are several types of beamformer methods (e.g., quiescent beamformer, linearly constrained minimum variance (LCMV) beamformer, and eigenspace-based beamformer). A mathematical computation of the LCMV is provided in Appendix A. Essentially, the LCMV beamformer applies a covariance matrix in order to suppress any interference from neighboring sources. Isolating regions of interest while suppressing interference from neighboring sources have also been utilized in other approaches. For example, bandpass filtering in the Fourier domain can isolate frequencies of interest within the EEG, while applying spatial low pass filters have been used to reduce interference from neighboring sources.

A related solution is to estimate the intracranial current densities associated with the electric potentials generated by active cortical pyramidal neurons. An example of source localization under this approach is the widely used low-resolution brain electromagnetic tomography (LORETA) and improved standardized low-resolution electromagnetic tomography (sLORETA) solutions (Pascual-Marqui et al., 2011; see Appendix A for details). sLORETA applies a statistical standardization of the current density values to scale cortical activity within a range of values. Groups of electrodes exhibiting similar cortical activity are clustered and displayed within a range of standardized values instead of a single source location. Despite their utility in estimating interictal spikes associated with SOZ foci (Song et al., 2015; Duez et al., 2019), a major limitation of both the LCMV and sLORETA approaches are that they (i) are computationally expensive and (ii) represent inverse estimates with non-unique solutions (i.e., source locations cannot be definitively determined using scalp data). Moreover, gradations in intensity from specific sources are difficult to view under these approaches because inverse methods only provide broad clusters of neural activity.

Here, we focus on monitoring both phase and energy of EEG signals in order to perform seizure localization. This method also has the potential to pin-point seizure occurrences on the cortex by the projected power of EEG signals and assuming a single source of power at a given instance in time. Existing methods of seizure location rely on the raw EEG analysis from an experienced clinician. Moreover, a robust automatic seizure location method should be sensitive, i.e., have high accuracy in locating all clinically locatable seizures and be reliable, i.e., have low false errors and not erroneously label non-seizure events (e.g., common EEG artefacts like eye-blinks, movements, etc.) as seizure occurrences. Thus, we compared our approach in its ability to distinguish true seizure events from other common artifacts of the EEG.

Our approach promotes the concept of quantitative EEG analysis (qEEG) to provide automated location based on neural markers. Spatial-temporal activity can be viewed as seizure activity producing an epicenter at the height of neural activity, as well as width varying gradations from the epicenter. The proposed method focuses on focal seizures that exhibit ~ 3 Hz activity and exhibit 5–10 times greater increase in amplitude from basal neural activity. Our method exploits the continuous analytic amplitude and phase information across EEG channels to robustly localize seizure foci on the scalp.

## 2. Methods

### 2.1. EEG data and preprocessing

This study used an existing, de-identified patient EEG database provided by the last author (J.W.W.), a board-certified pediatric neurologist specializing in epilepsy and its treatment, and Chief of Pediatric Neurology University of Tennessee Health Science Center (UTHSC). Original data collection protocols were approved by the UTHSC IRB (Protocol# 13-02783-XM). Raw EEGs were collected on an Electrical Geodesics Inc. (EGI) high-density EEG system. The dataset consisted of EEGs from  $N = 15$  patients (6 females, 9 males), who were, on average, ~20 years old. Patients in the sample were being treated at UTHSC for medically intractable epilepsy characterized by focal seizures consisting of abnormal hypersynchronous wave patterns.

EEG recordings included normal and abnormal (seizure) brain activity monitored for 60–90 minutes during examination, recorded at 128-channels according to the 10–20 system. Data were average referenced and sampled at 1000 Hz. Preprocessing included notch filtering to remove 60 Hz line noise and artifact removal whereby segments contaminated by myogenic noise and blinks ( $\pm 50 \mu\text{V}$ ) were automatically discarded using the algorithm described in the manuscript. Preprocessing was conducted using custom routines coded in MATLAB. In some instances, patient EEGs did not contain any seizure occurrences. This made it possible to first detect, and when present, locate seizure instances across channels. Confirmation of seizure location was provided by clinician judgments of J.W.W.'s neurology group.

Epileptic seizure occurrences were projected as synchronized oscillations with a specific frequency that was visible within a wide range of EEG channels. Fig. 1 shows a sample of how this type of seizure was observed in raw EEG data.

In order to find the most effective frequency band characterizing seizure episodes, we first calculated the Fast Fourier Transform (FFT) of the EEG signals within the time limit of a sample seizure occurrence. FFTs showed peak power at ~3 Hz and additional harmonic energy extending up to 11 Hz. We then determined the dominant frequency of seizure oscillations across all patients, which was between 2.7 to 2.9 Hz. Consequently, we band-pass filtered data to include this nominal frequency range that described seizure activity (1–15 Hz; transition bandwidth = 1 Hz;  $N = 370$ ). Peak-to-peak pass-band ripple was  $< 0.02$  dB, which guaranteed signal distortion of  $< 2\%$ . A  $\pm 2\%$  gain (0–20 Hz) and  $\pm 2\%$  distortion was achieved within the passband. Filtering was implemented in the EEGLAB MATLAB toolbox (<http://sccn.ucsd.edu/eeglab/>) (Delorme and Makeig, 2004) using the Parks-McClellan optimal finite impulse response (FIR) filter design method (McClellan and Parks, 1973).

### 2.2. Analytical amplitude method

Our seizure localization routines followed three main steps: (1) Hilbert Transform, (2) calculating the analytic amplitude and phase differences per channel, and (3) comparing these metrics across time/channels to determine the most likely seizure epicenter.

The proposed method first employed the Hilbert Transform to calculate the power and phase of the EEG signals. The Hilbert transform is defined as (Eq. (1)):

$$H(u_j(t)) = \frac{1}{\pi} PV \int_{-\infty}^{+\infty} \frac{V_j(t')}{(t-t')} dt' \quad (1)$$

where PV signifies the Cauchy Principal Value. The Hilbert transform is a linear operator like the FFT and is particularly appropriate for analyzing non-stationary signals by expressing frequency as a

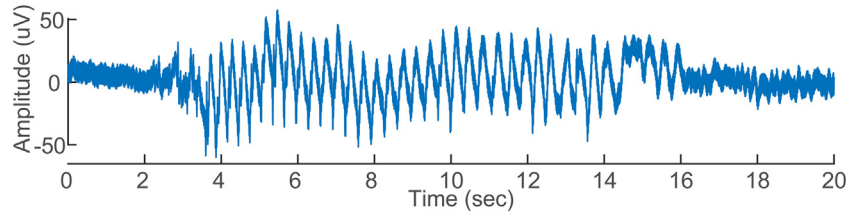


Fig. 1. An example of a seizure EEG waveform.

rate of change in phase. Calculating the Hilbert on all EEG signals yielded the analytical signals of each channel. The vector length at each digitizing step,  $t$  is the state variable for analytic amplitude. For each channel  $j$ , denoted as  $v_j(t)$  from the recorded EEG, the analytical signal,  $V_j(t)$  is a time series which consists of a real part,  $v_j(t)$  and an imaginary part  $u_j(t)$  which together form the complex number:  $V_j(t) = v_j(t) + iu_j(t)$ . The real part of the Hilbert transform is decomposed from the EEG signal to reflect the spatial ensemble average of the amplitude activity,  $v_j(t)$ , representing excitatory neurons,  $v(t)$  (Freeman, 2004). The Hilbert transform provides the imaginary part,  $u_j(t)$  of the signal representing an estimate of the output of the activity of inhibitory neurons (Freeman, 2004). The sum of squares of the real and imaginary parts of the signal produces the instantaneous power required by the excitatory and inhibitory neurons in local areas of the cortex from dendritic currents (Freeman, 2004). The analytic amplitude is calculated through the square root of that sum of values.

From the Hilbert output, we then calculated the time-varying Analytical Amplitude [ $A_j(t)$ ] and Phase signals [ $P_j(t)$ ] of the EEG for each channel  $j$  during the time period of seizure using Eqs. (2) and (3).

$$A_j(t) = \sqrt{v_j^2(t) + u_j^2(t)} \quad (2)$$

The square root of the sum of the squares from the real and imaginary parts of the signal produces the Analytical Amplitude  $A_j(t)$ .

$$P_j(t) = \tan^{-1}\left(\frac{u_j(t)}{v_j(t)}\right) \quad (3)$$

The arctangent of the real and imaginary parts of the signal produce the Analytical Phase  $P_j(t)$ .

The phase difference at every instant was then computed by differentiating the consecutive phase values at every sample (Eq. (4)).

$$\Delta P_j(t) = P_j(t) - P_j(t-1) \quad (4)$$

We could not rely solely on the instantaneous values of Analytical Amplitude and Phase to locate the occurrence of seizures, due to spurious noise, movement and artefacts that may produce false-positives. Thus, a weighted summation function of the Analytical Amplitude and Phase Differences within a fixed time window acted as a memory function to predict if the specific period of data was representative of a seizure occurrence. Two indices were introduced to quantify the resemblance of signal to the seizure. The first index operates on the Analytical Amplitude ( $S_{AAj}$ ) and the second on the Analytical Phase Difference ( $S_{APj}$ ):

$$S_{AAj}(t) = \sum_{k=0}^M e^{-\lambda k} A_j(t-k) \quad (5)$$

$$S_{APj}(t) = \sum_{k=0}^M e^{-\lambda k} \Delta P_j(t-k)$$

where  $\lambda$  is the forgetting factor,  $M$  is the length of the window and their values determine the degree in which past data would affect the indices. The received signal  $t$  is subtracted from the transmitted

signal  $k$ . These values were selected to filter out the transient effect of common artefacts on the analytical amplitude and phase signals that would typically last for several seconds. The weighted summation function was based on the recursive least-squares algorithm with an adaptive forgetting factor for optimal filtering. If the forgetting factor  $\lambda$  is large, the function has a long time series length to reduce the effects of spurious noise; if the forgetting factor  $\lambda$  is small then the function is adapted to the channel dynamics and can identify artefacts such as seizure instances (Zhuang, 1998). The weighted summation function is applied to the Analytical Amplitude [ $A_j$ ] and Phase Differences [ $\Delta P_j$ ]. Values of both indices were then compared to data driven patient specific thresholds to locate the seizure occurrences.

Because differences between seizure occurrences exist across patients, a fixed threshold could not be used for all individuals. We used the following formulation to scale individual threshold values:

$$SA_{threshold} = X \times SD_{patient} \quad (6)$$

$$SP_{threshold} = Y$$

The values of coefficients ( $X$ ,  $Y$ ) were chosen experimentally by analyzing and comparing the patterns of changes for different occurrences of seizures and artefacts and selecting the most appropriate value. In order to compensate for cross-patient differences in signal amplitudes, we measured the standard deviation of a period of EEG data for each subject ( $SD_{patient}$ ) and used that value to scale the thresholds for each patient. It should be noted that only the amplitude threshold ( $SA_{threshold}$ ) was variable between patients. In addition, differences between the two coefficients were due to the fact that  $SP_{threshold}$  was being compared to the phase differences, which tended to be small as compared to amplitude values. The algorithm was set to recognize seizure occurrences only when both conditions were met for a region of interest (ROI) of EEG channels:

$$S_{AAj} > SA_{threshold} \quad (7)$$

$$S_{APj} > SP_{threshold}$$

The Analytical Amplitude ( $S_{AAj}$ ) and the Analytical Phase Difference ( $S_{APj}$ ) values greater than the threshold would signify a vector of channels that exhibit synchronous, low frequency ( $\sim 3$ Hz), and high amplitude behavior.

### 2.3. Seizure localization

Having located seizure occurrences within the time dimension (Fig. 2a), our next step was to find the most probable location of its occurrence. Assuming that a seizure is caused by a single source located on the cortex of the brain, we reasoned we could localize seizure activity by finding a constant value appearing through several consecutive channels across a phase difference diagram (see Fig. 2c). Initially, we examined the analytic phase of all channels within a time sequence spanning the occurrence of a seizure event, and expected to see unified low frequency, high amplitude EEG energy during seizure states. We measured the corresponding

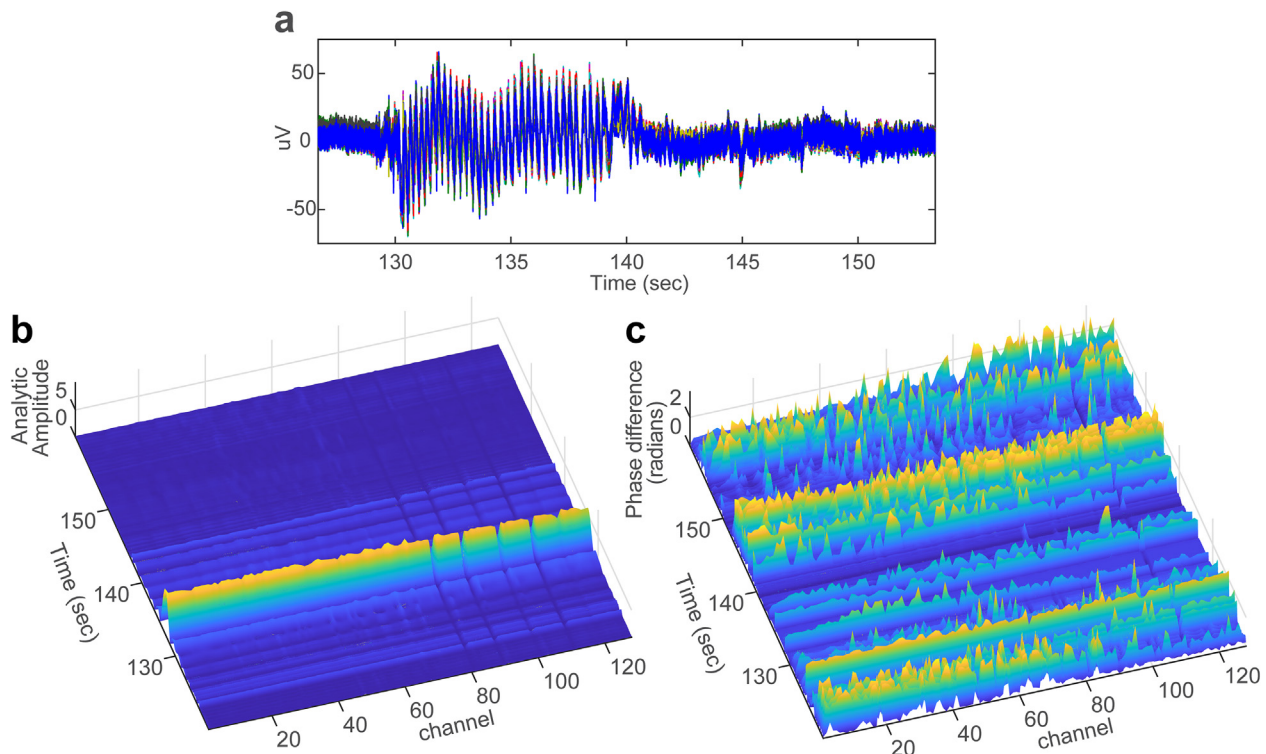


**Fig. 2.** (a) Seizure activity from multiple channels, (b) analytic amplitude and (c) phase.

maximum analytical amplitude values within the period of seizure (see Fig. 2b). We used the analytical amplitude values from that instant to find the channel with the maximum value.

Analytic amplitudes were then sorted in time and cross-correlated to the channel vector which holds a row of analytic amplitudes per time segment. For all time segments, the maximum analytic amplitude was found, which was taken as the estimated epicenter of seizure intensity at that time instance.

The following steps summarize our seizure localization routine:

- i. Select EEG data with seizure occurrences for processing
- ii. Apply Eqs. (2)–(7).
- iii. Sort AA values with time, in order to associate associating highest AA to a time instance.
- iv. Find max AA value among all channels
- v. Cross-correlate AA index value in channel vector/electrode value with time instance.

The final output provided the location (channel) and time instance with highest AA value associated with seizure activity.

### 3. Results

#### 3.1. Analytic amplitude and phase descriptions of seizure EEG

When present, seizure activity was identified as a clear boundary from low-amplitude, asynchronous activity to high-amplitude, rhythmic activity, where small changes in excitatory synaptic gain led to strong oscillatory activity. Among 128 electrodes, we found seizure activity were robust in Less or equal to 25 channels (~20% of electrodes). All 15 patients had focal seizures whose abnormal neural behavior was observable in their EEG. Fig. 2b shows how the analytic amplitude and phase difference (Fig. 2c) of the signal changed during the seizure period across all channels and time. Seizure oscillations manifested as an almost sinusoidal signal with

a frequency of  $\sim 3$  Hz and abnormal changes in power. Phase changes of the signal also became more organized, causing the phase difference diagram to transform from completely random changing values to small constant values that lingered for as long as the seizure event. The standard deviation across channels of the phase differences provided plateaus of low values punctuated by spikes of the analytic amplitude.

Fig. 2a demonstrates the localized power of a seizure event across all electrodes at a single time instance. The phase of a signal that is approaching periodic behavior could be represented as continually increasing, and if there were two signals having the same sign, they would be reinforcing each other, whereas the phase difference between them would approach zero. We see the phase differences approached zero in Fig. 2c during the seizure instance due to the semi-periodic behavior of the EEG during aberrant events. This instance is concentrated due to the phase differences of neighboring semi-periodic behaving signals.

#### 3.2. Distinguishing seizure activity from EEG artifact

Another important challenge was to distinguish between EEG artefacts and true seizure events. Our method could effectively rule out common artefacts like bad electrode contacts and muscle or eye movements because these artefacts are usually time limited, are aperiodic, and do not induce phase synchronization. Fig. 3 depicts this difference projected on the calculated Analytical Phase Index from Eq. (5). Fig. 3a shows a typical artefact (i.e., voluntary head movement). Similarly, Fig. 3b demonstrates the analytic amplitude and Fig. 3c demonstrates the phase differences observed in artefact instances. The phase differences of seizure instances approach zero (depicted in blue in Fig. 2c) since neighboring electrodes exhibit the same semi-periodic behavior as opposed to the phase differences of the artefacts which exhibit non-zero random values in Fig. 3c.

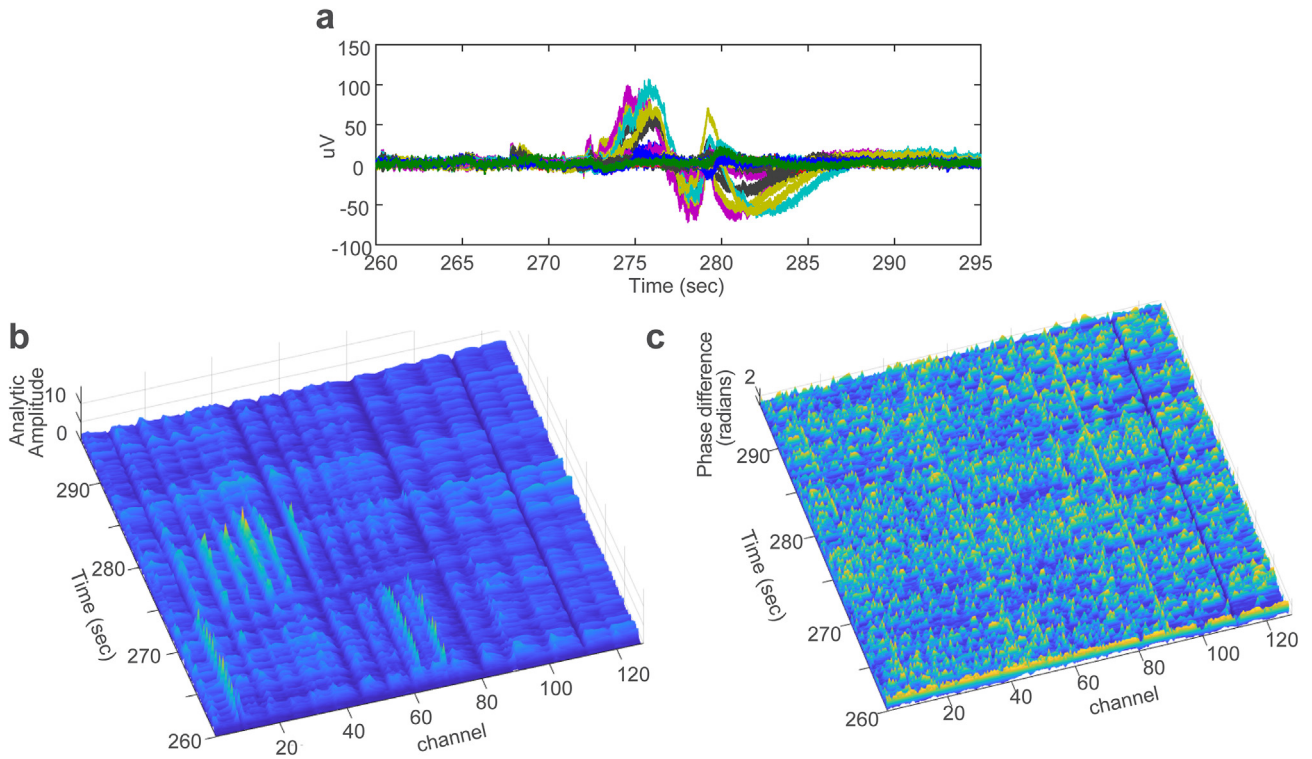


**Fig. 3.** (a) Artefact activity from multiple channels, (b) analytic amplitude and (c) phase.

The Analytical Phase Index (Eq. (5)) shows a clear period of synchronization for the seizure event across all channels, while an artefact exhibits a sudden change in the amplitude synchronization observed briefly, and dissipates much faster than a seizure event. By choosing the appropriate threshold (Eq. (6)) we could successfully rule out the artefacts by the location method itself. This capability of our method removes the need for further preprocessing for artefact removal which becomes an important limitation when the algorithm is desired to work in real-time.

Fig. 4 shows changes in the analytic amplitude of the signal during the occurrence of seizures. The relative distance of the source from each channel is apparent. Fig. 4a illustrates changes through time of the peak of the seizure location temporally. A 2-dimensional display of the analytic amplitude with time on the y-axis and channel/electrodes on the x-axis provides an overview of the intensity of the seizure as the higher amplitudes cluster around a group of channels. A magnified view shown in Fig. 4b demonstrates how peak seizure occurrence concentrates into con-

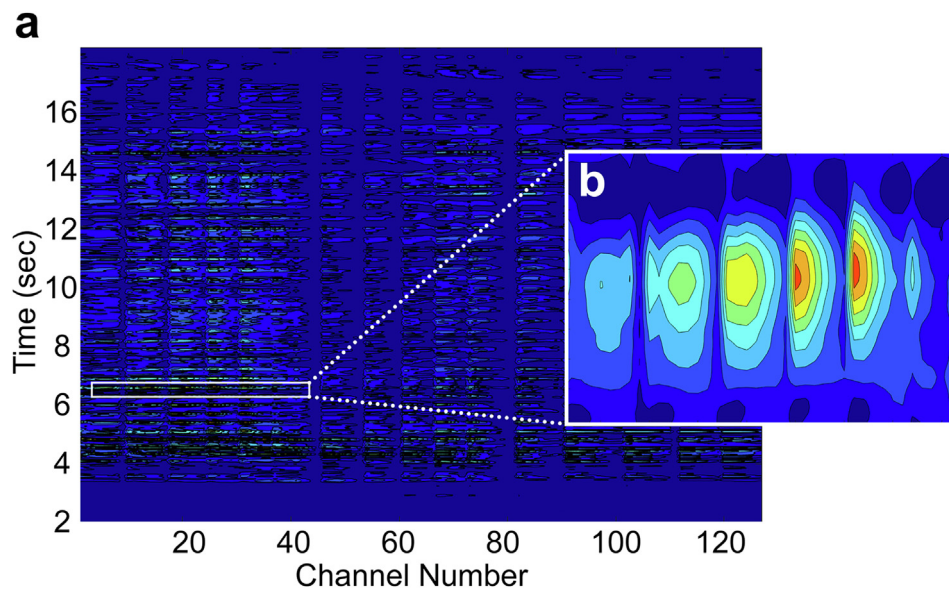


**Fig. 4.** Visualization of the Analytical Amplitude changes within the time period of the seizure occurrence. (a) Complete time range, (b) zoomed view. The peak seizure occurrence is found in in the Analytical Amplitude which concentrates into concentric circles and then slowly dissipates over time.

centric circles and then slowly dissipates. Varying gradients of amplitude intensities can be seen in this magnified view.

### 3.3. Comparison of algorithm performance with other methods

Our EEG data consisted of time instances of seizures and artefacts. The number of artefacts existing in the data and the percentage of false positive seizure detections were assessed to examine how robust our method is in deciphering seizure occurrences vs. artefacts. EEG datasets were separated into possible seizure events and processed through our methodology. Most patients exhibited frontal lobe seizure activity (9/15). In some instances, more than one seizure event was detected in their EEG time series. The average duration of seizures was 10.8 sec. Our blinded source location results were then confirmed against expert clinical judgements of Dr. Wheless' group.

We found the proposed algorithm achieved 93.3% precision and accuracy and 100% sensitivity in seizure detection. The specificity (true negative rate) was 0%, i.e., the algorithm produced no true negatives. Additionally, only 6% of EEG data resulted in false locations. Results from the localization analysis are summarized in Table 1. Chi Squared Goodness of Fit was performed to determine how empirically determined electrode locations compared to physician observed seizure locations. Calculated electrode locations showed excellent agreement with clinical judgements ( $X^2 = 0.044$ ,  $P = 1.000$ ). Our seizure location algorithm could not precisely locate one of the seizure locations (Patient 6). The false positive the algorithm produced may be due to the cluster occurrences in multi-focal locations, such that seizure activity was found in a cluster (F1, F3, F5, FC1, FC3 and FC5) vs. an epicenter.

As a further validation test, we compared our proposed algorithm of seizure localization to the well-known beamformer approach (for details, see Appendix A). The eigenspace-based beamformer algorithm achieved 73.3% precision and accuracy and 100% sensitivity. Only 11/15 seizures were located. The specificity or true negative rate was 0% (i.e. the algorithm produced no true negatives). Additionally, only 27% of the EEG seizure data set resulted in false locations. Results from the localization analysis are summarized in Table 2. The empirically determined electrode foci agreed with clinical judgments ( $X^2 = 1.298$ ,  $P = 0.999$ ). The false positive of the algorithm may again be due to cluster occurrences in multi-focal locations in some patients including Patient 6, Patient 4 (left centroparietal), Patient 5 (right posterior temporal), and Patient 11 (POz, FT7, P4, Cz).

**Table 1**  
Results from the seizure localization.

Patient	Gender	Age	Seizure Location	TP/FP
1	M	15	T9	TP
2	F	21	F5	TP
3	M	17	P5	TP
4	M	22	CP1, FT10	TP
5	M	20	P8	TP
6	M	20		FP
7	F	15	Oz	TP
8	F	14	FT9, F10	TP
9	F	38	FT8	TP
10	F	19	C4	TP
11	F	21	POz, FT7, P4, Cz	TP
12	M	15	F8, T4	TP
13	M	17	Fp2	TP
14	M	21	F3	TP
15	M	20	Fp1	TP

\*TP (true positive) and FP (false positive), M (male), F (female).

**Table 2**  
Results from the seizure localization – Beamformer.

Patient	Seizure Location	TP/FP
1	T9	TP
2	F5	TP
3	P5	TP
4		FP
5		FP
6		FP
7	Oz	TP
8	FT9, F10	TP
9	FT8	TP
10	C4	TP
11		FP
12	F8, T4	TP
13	Fp2	TP
14	F3	TP
15	Fp1	TP

### 3.4. Epicenter localization

A 3D visualization of the topography of analytical amplitude across the scalp is shown in Fig. 5. Maximum analytic amplitude was taken as the epicenter of seizure intensity at a time instance. As seen in the representative patient in Fig. 5, localized seizure instances are observed with varying degrees of lesser intensities over the scalp. Results show that channel 22 (Fp1) is the source of the highest seizure activity, with neighboring channels 21 and 26. Neighboring electrodes exhibit varying gradations of color intensity, highlighting the focal point of seizure activity (dark red), and varying levels of lower intensities around the focal point.

## 4. Discussion

We present a new approach to localizing seizure-related neural activity from EEG recordings based on analysis of analytic amplitude and phase differences over time and across channels. Results revealed localized epicenters of low frequency, high energy neural activity. Our method was robust in locating relatively short seizure instances (8–12 seconds) and achieved 93.3% precision and accuracy and 100% sensitivity in detecting true seizure activity from ongoing EEG and common artifacts.

EEG data showed that seizure activity was largely restricted to a bandwidth of periodic activity at ~3 Hz. Internally modulated neural activity is maintained through the self-organization amongst excitatory cortical neurons and inhibitory neurons (Freeman, 1975; 2004). When mutual inhibition exceeds that of mutual excitation, an oscillation repeats a complex pattern about every 0.3 s (Freeman 1972). Freeman has found through electrical stimulation of the lateral olfactory tract (LOT) in the prepyriform cortex (PC) of the cat, rat and rabbit models that seizures are induced that exhibit dominant localized oscillatory behavior (Freeman 1962, 1972). Biologically based models have been developed to capture the dynamics of localized seizure behavior and explain the dynamics of local and global neural networks (Freeman 1972, Kozma and Freeman 2001, Myers and Kozma, 2018). Dominant delta neural activity (~3 Hz) has been exhibited in which some inhibitory neurons become more disinhibited (excited) and others more inhibited (less active) (Freeman, 1986). If inhibitory neurons gain in intensity, thereby inhibiting their neighbors, excited regenerative feedback produces an explosive discharge. This result in an inhibitory post-synaptic potential in the excitatory neurons to which they are projected (Freeman et al. 2006). Seizure instances are sustained losses of mutual competitive activity that can manifest into explosive growth of local activity (Freeman et al. 2006).

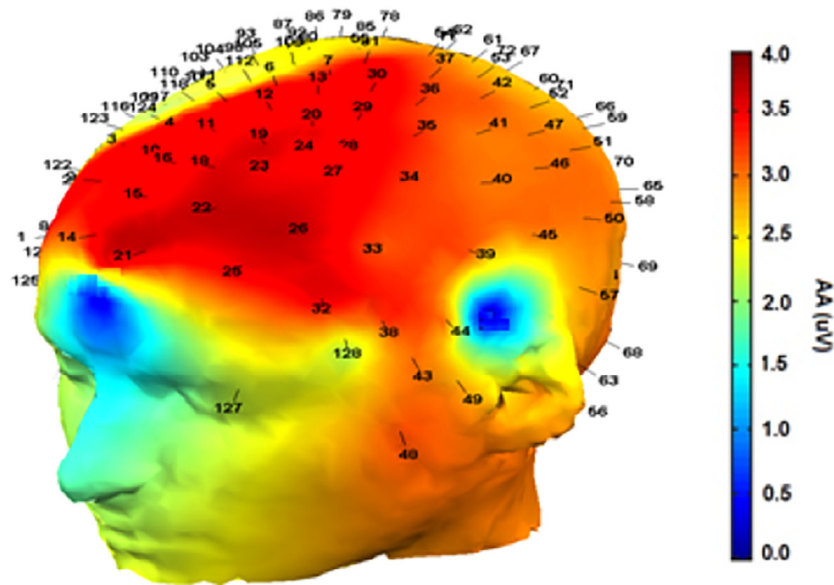


Fig. 5. Map of localization results using the Analytical Amplitude of EEG signals (Patient 15).

Our technique reveals that localized neural behavior can be captured through signal decomposition (Hilbert amplitude and phase). The Hilbert transform provides temporal resolution of the near-instantaneous amplitude and phase (Freeman, 2004) and differentiated localized electrode intensities with the appropriate choice of band pass filter to isolate seizure activity. The inverse relationship demonstrated in Fig. 2 of the phase differences and analytic amplitude confirms previous studies using the Hilbert and Fourier techniques (Freeman, 2006).

Another important property of our approach is that it cleanly differentiated aberrant neural activity of interest (seizure events) from common EEG artifacts. Our algorithm performed with 93.3% precision and accuracy and 100% sensitivity in segregating true seizure events. When random movements are produced that contribute to artefacts, phase differences produce non-zero random values (Fig. 3) and there is little coherence across neural neighboring areas. Compared to seizure events, we found that phase differences can distinguish seizure instances that are relatively short term due to the high coherence of neural activity among neighboring electrodes. The high-temporal resolution of our approach resolves the semi-periodic behavior of seizure instances, as brief as several seconds.

The epicenter of seizure activity is also highlighted through implementation of our novel algorithm. As neural activity transitions to seizure behavior, neural spiking activity increases across spatial and temporal instances. These events may also involve electromyographic activity (e.g., appendage and face movement) that can confound EEG recordings. In this regard, implementing a weighted summation function [Eq. (5)] helped eliminate true negatives and reduced artefact occurrences. The analytic phase and amplitude approach compared favorably to the beamformer methodology in terms of artefact and noise suppression. Seizure thresholds were applied (Eqs. (6) and (7)) in order to distinguish seizure activity from background neural activity. The temporal changes of the epicenter of the seizure intensity are also visible using our method (Figs. 4 and 5). Our approach shows that maximum analytic amplitude can be used to determine the epicenter of seizure intensity on the scalp. Still, the effects of high-amplitude seizure instances are both localized and have gradient effects that are far reaching across the head (Fig. 5). As an analogy,

similar effects would be expected during earthquake events near the epicenter.

Other source localization methods have been proposed in the literature (see Appendix A) and have been used to localize seizure activity with variable success. The eigenspace-based beamformer, for example, is superior to both the quiescent and the LCMV beamformer, as it combines a low white noise gain with a high suppression of the interfering source. However, the quiescent beamformer does not succeed in suppressing interfering 15 Hz source activity (Muthuraman et al., 2014). The eigenspace-based beamformer strongly suppresses interfering sources, yet it still maintains a low white noise gain. Additionally, the output signal of the eigenspace beamformer has slightly lower amplitude than the original source activity (Muthuraman et al., 2014). Similarly, LORETA source estimate errors can be measured by taking the distance between the location of the absolute maximum value ( $|z_i|$  or  $||J_i|$ ) and the actual location of the test source (Pascual-Marqui et al., 2011). The related sLORETA algorithm shows zero localization error under ideal (no-noise) conditions as compared to the LORETA method (Pascual-Marqui, 2002; 2011). Still, a major limitation of both the LCMV and LORETA approaches are that they are computationally expensive and represent inverse estimates with non-unique solutions (i.e., source locations cannot be definitively determined using scalp data). Our “analytic signal” method performs well under ‘ideal’ and realistic noise conditions, considering that it was tested in noisy, biologically-based systems (i.e., real patients). Yet, our approach maintains a high precision, accuracy, and sensitivity rate while robustly localizing seizure activity at the scalp—which does not require the assumptions assumed by the aforementioned inverse source methods.

## 5. Conclusions

We developed a novel method to localize seizure-related activity using scalp EEG based on the Hilbert Transform and analytic amplitude/phase of neural signals. Empirical analysis on clinical seizure EEG data showed the proposed method is effective for fast and reliable localization of seizure activity. The method is applicable to seizures located in the cortex vs. seizure occurrences due to

substructures within the brain where EEG and MRI techniques have been utilized. The algorithm achieved high precision, accuracy and sensitivity rates of localization due to optimal filtering and the introduction of a weighted summation function that reduced extraneous artefacts from the signal. The method was found to be robust in locating relatively short seizure instances (8–12 seconds), usually considered as intractable types of seizures where surgery and medication cannot be utilized. Our method may offer a new approach to aid clinicians in localization of seizure activity. Future studies are needed to determine the utility of the method to offer seizure diagnostics in real-time.

## Acknowledgements

G.M.B. was partially supported by NIH/NIDCD R01DC016267.

## Appendix A

### A.1. Linearly constrained minimum variance (LCMV) beamformer

Van Hoey et al. (1999) discusses the forward problem in the calculation of potentials measured at the scalp electrodes caused by a known electrical dipole source within the head. The following equation determines the potential distribution of the scalp electrodes and their respective dipoles and its components, with  $c \in \mathbb{R}^{m \times 1}$ :

$$c = L(r_d) \times d \quad (\text{A1})$$

The parameters of the dipole are its coordinates in  $r_d$  and its dipole components in  $d$  (Van Hoey et al., 1999). The lead field matrix,  $L$  is determined by dipole position, electrode positions, and head geometry. A beamformer with the smallest additive white noise gain is called the quiescent beamformer (Van Hoey et al., 1999).

$$w_Q c (c^T c)^{-1} \quad (\text{A2})$$

The linearly constrained minimum variance (LCMV) beamformer, is more sensitive to white noise than the quiescent beamformer. The (LCMV) beamformer requires the weight vector to minimize the output power (Van Hoey et al., 1999):

$$\min_w w^T R_v w \quad s : t : w^T c = 1 \quad (\text{A3})$$

The (LCMV) beamformer:

$$w_{LCMV} = R_v^{-1} c (c^T R_v^{-1} c)^{-1} \quad (\text{A4})$$

where the matrix  $R_v$  will be calculated from the measurement of the EEG during the time interval:

$$R_v = \frac{1}{n} V^T V \quad (\text{A5})$$

where  $V \in \mathbb{R}^{m \times n}$ ; and the EEG signal is measured at  $m$  electrodes during  $n$  time samples by the matrix (Van Hoey et al., 1999). The covariance matrix  $R_v$  enables the determination of the weights in  $w$  while suppressing any interference from neighboring sources. In this manner, the LCMV beamformer can reduce the interference from the contribution of the local potential distributions from the area of interest.

The eigenspace-based beamformer divides the  $m$ -dimensional measurement space into signal space and a noise space, based on  $V$  (Van Hoey et al., 1999).

$$V = P^T S Q; P R^{m \times m}; Q R^{n \times n}; \quad (\text{A6})$$

The diagonal matrix  $S$  contains the number of dipolar sources which should be equal to the noise variance. The corresponding columns  $P$  are a set of basis vectors that span the signal space and  $Q$  are a set of basis vectors that span time (Van Hoey et al., 1999).

### A.2. LORETA and sLORETA

The low-resolution brain electromagnetic tomography (LORETA) solution uses a non-weighted minimum norm solution (Pascual-Marqui et al., 2011):

$$J = K^T (K K^T + \alpha H)^+ \varphi. \quad (\text{A7})$$

where  $K = H K_c$ , given the lead field  $K_c$ , and matrix  $H$  which is known in statistics as the centering matrix. The superscript '+' denotes the Moore–Penrose pseudoinverse (Rao and Mitra, 1973) where  $\alpha \geq 0$  is known as the Tikhonov regularization parameter (Tikhonov et al., 1995). The term, ' $\varphi$ ' comes from  $\varphi = H \varphi_c$ , where  $\varphi_c \in \mathbb{R}_E^{N_E}$  denotes the potentials at  $N_E$  scalp electrodes.

An improved approach known as standardized low-resolution electromagnetic tomography (sLORETA) involves a post-processing statistical standardization of the current density values (Pascual-Marqui, 2002; 2011):

$$z_i = \frac{[J]_i}{[S_j]_{ii}^{1/2}} \quad (\text{A8})$$

where  $[J]_i$  is the estimated current density at the  $i$ th voxel;  $S_j \in \mathbb{R}^{N_v \times N_v}$  is the covariance matrix for the current density at  $N_v$  cortical voxels; and  $[S_j]_{ii}$  is its  $i$ th diagonal element corresponding to the variance at the  $i$ th voxel (Pascual-Marqui et al., 2011).

## References

- Boon P, D'Havé M, Adam C, Vonck K, Baulac M, Vandekerckhove T, Reuck JD. Dipole modeling in epilepsy surgery candidates. *Epilepsia* 1997;38(2):208–18.
- Boon P, D'Havé M. Interictal and ictal dipole modelling in patients with refractory partial epilepsy. *Acta Neurol Scand* 1995;92(1):7–18.
- Delorme A, Makeig S. EEGLAB: an open source toolbox for analysis of single-trial EEG dynamics including independent component analysis. *J Neurosci Methods* 2004;134(1):9–21.
- Duez L, Tankisi H, Hansen PO, Sidenius P, Sabers A, Pinborg LH, et al. Electromagnetic source imaging in presurgical workup of patients with epilepsy: A prospective study. *Neurology* 2019;92:e576–86.
- Freeman WJ. Alterations in prepyriform evoked potential in relation to stimulus intensity. *Exp Neurol* 1962;6:70–84.
- Freeman WJ. Waves, pulses and the theory of neural masses. *Progr Theor Biol* 1972;2:87–165.
- Freeman WJ. Mass Action in the Nervous System. New York: Academic Press; 1975.
- Freeman WJ. Origin, structure, and role of background EEG activity. Part 1. Analytic amplitude. *Clin Neurophysiol* 2004;115(9):2077–88.
- Freeman WJ. Origin, structure, and role of background EEG activity. Part 4 Neural Frame Simulation. *Clin Neurophysiol* 2006;117:572–89.
- Freeman WJ. Petit mal seizure spikes in olfactory bulb and cortex caused by runaway inhibition after exhaustion of excitation. *Brain Research Reviews* 1986;11(3):259–84.
- Freeman WJ, Holmes MD, West GA, Vanhatalo S. Dynamics of human neocortex that optimizes its stability and flexibility. *Int J Intell Syst* 2006;21:1–21.
- Hartmann MM, Furba F, Perko H, Skupch A, Lackmayer K, Baumgartner C, et al. EpiScan: online seizure detection for epilepsy monitoring units. In 2011 Annual International Conference of the IEEE Engineering in Medicine and Biology Society 2011:6096–9.
- Kozma R, Freeman WJ. Chaotic resonance—method and applications for robust classification of noisy and variable patterns. *Int J Bifurc Chaos* 2001;11:1607–29.
- McClellan J, Parks T. A unified approach to the design of optimum FIR linear-phase digital filters. *IEEE Trans Circuit Theory* 1973;20(6):697–701.
- Michel CM, Murray MM, Lantz G, Gonzalez S, Spinelli L, de Peralta RG. EEG source imaging. *Clin Neurophysiol* 2004;115(10):2195–222.
- Muthuraman M, Hellriegel H, Hoogenboom N, Anwar AR, Mideksa JG, Krause H, Raethjen J. Beamformer source analysis and connectivity on concurrent EEG and MEG data during voluntary movements. *PLoS One* 2014;9(3): e91441.
- Myers MH, Kozma R. Mesoscopic neuron population modeling of normal/epileptic brain dynamics. *Cogn Neurodyn* 2018;12(2):211–23.

- Pascual-Marqui RD. Standardized low-resolution brain electromagnetic tomography (SLORETA): technical details. *Methods Find Exp Clin Pharmacol* 2002;24(Suppl D):5–12.
- Pascual-Marqui RD, Lehmann D, Koukkou M, Kochi K, Anderer P, Saletu B, et al. Assessing interactions in the brain with exact low-resolution electromagnetic tomography. *Philos Trans A Math Phys Eng Sci* 2011(369):3768–84.
- Rao CR, Mitra SK. Theory and application of constrained inverse of matrices. *SIAM J Appl Math* 1973;24(4):473–88.
- Shoeb A, Edwards H, Connolly J, Bourgeois B, Treves ST, Gutttag J. Patient-specific seizure onset detection. *Epilepsy Behav* 2004;5(4):483–98.
- Shoeb AH, Gutttag JV. Application of machine learning to epileptic seizure detection. In: *Proceedings of the 27th International Conference on Machine Learning (ICML-10)* 2010 (pp. 975–982).
- Song J, Davey C, Poulsen C, Luu P, Turovets S, Anderson E, et al. EEG source localization: Sensor density and head surface coverage. *J Neurosci Meth* 2015;256:9–21.
- Tikhonov AN, Goncharsky AV, Stepanov VV, Yagola AG. *Numerical Methods for Solving Ill-Posed Problems*. Translation: Hoksbergen RAM (Kluwer, Boston). 1995.
- Van Hoey G, Van de Walle R, Vanrumste B, D'Havse M, Lemahieu I, Boon P. Beamforming techniques applied in EEG source analysis. *Proc ProRISC99* 1999;10:545–9.
- Westmijse I, Ossenblok P, Gunning B, Van Luijckelaar G. Onset and propagation of spike and slow wave discharges in human absence epilepsy: a MEG study. *Epilepsia* 2009;50(12):2538–48.
- Zhuang W. RLS Algorithm with Variable Forgetting Factor for Decision Feedback Equalizer over Time-Variant Fading Channels. *Wirel Pers Commun* 1998;8(1):15–29.